

Reinforcement and environmental degradation of nylon-6/clay nanocomposites

J.S. Shelley^a, P.T. Mather^b, K.L. DeVries^{c,*}

^a*Air Force Research Laboratory, Propulsion Directorate, Edwards AFB, CA 93551, USA*

^b*Institute of Materials Science and Chemical Engineering Departments, University of Connecticut, Storrs, CT 06269, USA*

^c*Department of Mechanical Engineering, 2220 Merrill Engineering Building, University of Utah, Salt Lake City, UT 84112, USA*

Received 1 May 2000; received in revised form 1 December 2000; accepted 6 December 2000

Abstract

Hybrid organic/inorganic nanocomposites are being developed to improve the physical and mechanical properties of polymeric materials without adversely effecting their processing characteristics. One such nanocomposite developed by Toyota and commercialized by Ube Industries is the nylon-6/montmorillonite clay nanocomposite. The mechanism of reinforcement in nylon-6/clay nanocomposite materials is investigated through tensile experiments, infrared absorption spectrography, and dynamic mechanical analysis. 200% improvements in modulus and 175% improvements in yield stress are attributed to the complexation of mid-chain carbonyl groups with the exfoliated clay lamellae. Because of the initial use of these materials in automotive components, and the known deleterious effects of the air pollutant NO_x on nylon-6, the degradation of the nanocomposites in NO_x was examined through post-exposure tensile experiments. It was found that NO_x degrades the mechanical performance of the nanocomposites regardless of the constraining effect of clay lamellae. © 2001 Elsevier Science Ltd. All rights reserved.

Keywords: Nylon-6/clay nanocomposites; Hybrid polymers; NO_x degradation

1. Introduction

Studies by researchers at Toyota have demonstrated a 168% increase room temperature tensile modulus, an 87°C increase in heat distortion temperature (HDT) [1], and a 40% decrease in water permeability [2] of nylon-6/clay nanocomposites over unmodified nylon-6. These property improvements are attributed to a significant volume of polymer chains constrained by their interaction with the exfoliated clay lamellae. Specifically, over 30% of the material volume may be accounted for in these constrained regions of 5 wt% clay reinforced nylon-6. While the end groups of modified nylon-6 chains are ionically bonded to the clay lamellae [3], this interaction alone does not account for the magnitude of the constrained region or the preference of the nanocomposites for the gamma crystal phase [4]. The nature of the constrained region as the mechanism of reinforcement has yet to be satisfactorily explained and property improvements have yet to be confirmed on commercially available nanocomposites using standard processing techniques.

Although one of the first applications of these materials is in under-the-hood components in automobiles [5], and NO_x is a pollutant in automobile exhaust that is known to have deleterious effects on the mechanical properties of nylon-6 [6], no information exists in the literature on the effects of NO_x on the properties of the nanocomposite materials. NO_x degradation of nylon-6 is a chemical-kinetic process that may not be diffusion limited. Therefore, the decrease in diffusion through the nanocomposite materials may not protect them from NO_x degradation.

Considering the dimensions of polymer chains and their crystalline assemblies, it can be said that all polymers have structure on the nanometer size scale and, further, that the mechanical properties of polymers are governed by the interactions of these “nanostructures” with one another. Therefore, to influence the interactions that govern the mechanical properties of polymers, specific nano-scale reinforcement is efficient and beneficial. Montmorillonite clay provides such reinforcement through the interaction of nylon-6 polymer chains with the charged surfaces of clay lamellae. The lamellae are phyllosilicate platelets nominally 1 nm thick and 100 nm square uniformly dispersed throughout the nylon-6 matrix [5]. Isomorphous substitution of aluminum or iron atoms of valence 3 for the silicon atoms

* Corresponding author. Tel.: +1-801-581-7101; fax: +1-801-585-8692.
E-mail address: larry.devries@dean.eng.utah.edu (K.L. DeVries).

of valence 4 in the tetrahedrally bonded Si_2O_5 silicate monolayers in the naturally occurring mineral leaves the clay lamella with a net negative charge [7]. The negative charge is balanced by sodium or calcium ions in the galleries between the lamellae in the mineral, which exhibit a cation exchange capacity of 119 meq/100 g for intercalated sodium.

The hybridization process published by the Toyota researchers uses either 12-aminolauric acid or ϵ -caprolactam in HCl to cationically exchange the sodium ions. ϵ -caprolactam monomer is then able to permeate the aluminum silicate layers and polymerize by ring opening catalyzed by 6-aminocaproic acid. The result is an exfoliated nylon-6/clay nanocomposite in which ionized 12-aminolauric acid ammonium end groups interact with the charged clay lamella surface. It is this ion exchange capacity and net negative charge on the clay lamellae that permits ionic bonding between the clay lamellae and modified ammonium chain ends of the nylon-6 [8].

The interaction of polymer chains with montmorillonite has been known for over forty years. In March 1958, E.A. Hauser was issued a patent for “clay complexes with conjugated unsaturated aliphatic compounds of four to five carbon atoms” [9]. The spontaneous polymerization of butadiene and 4-vinyl pyridine on montmorillonite surfaces with an “ionic mechanism of polymerization” [10] was studied as early as 1963. The US patents for the nylon-6/clay materials were issued in 1988 [11] referencing the Japanese patents from 1985 and 1986. Other patents were issued as early as 1980 for intercalated montmorillonite/vinyl and montmorillonite clay composites with a “strong chemical bond” between the clay surface and organic polymer [12].

Other polymers have been intercalated and hybridized with montmorillonite lamellae with varying degrees of success. Similar trends as reported by the Toyota researchers, but with significantly less dramatic results, have been reported for in-situ polymerized nanocomposites of nylon-6 and surface modified silica particulates [13]. Like the Toyota researchers, Yang, et al. found that the property improvements showed a maximum at a 5 wt% loading. Polypropylene has been intercalated using stearyl ammonium as the ion exchange molecule and maleic anhydride modified polypropylene as a compatibilizer [14,15]. Glass transition temperature decreases slightly with clay incorporation, but room temperature storage modulus increases by 159%. PET/clay hybrids [16] exhibit improved HDTs and elastic moduli with slightly reduced melting temperatures. A PMMA/clay hybrid was produced via emulsion polymerization [17] with improved modulus and yield strength, but significantly reduced strain at yield. The Toyota researchers have also developed polyimide/clay nanocomposites using dodecylamine in HCl to ion exchange and disperse the clay in dimethylacetamide [18]. Lan et al. [19] determined that the number of methylene units in the ion exchange amine influenced the ability of the clay to be intercalated and exfoliated by the polymeriza-

tion of polyamic acid. The permeability of polyimide hybrid nanocomposites to CO_2 decreases non-linearly with increasing clay content. Protonated 12-aminododecanoic acid serves as the intercalation molecule for poly(ϵ -caprolactone) hybrids [20] that exhibit significantly reduced water permeabilities. Epoxy resins self-polymerize and exfoliate the clay lamellae in the presence of ion exchanged montmorillonite [21]. Most of these materials were created only on the laboratory scale and research tends to center on proof-of-exfoliation of the clay into a hybrid nanocomposite morphology through X-ray analysis. Unfortunately, the mechanism of mechanical property improvement is rarely discussed.

2. Experimental

2.1. Tensile

As received pellets were dried in under house vacuum for at least 2 h before being extruded through a Randcastle 1/2 single screw extruder with sheet dye using a 4:1 draw ratio. The resulting extruded sheet was 0.3 ± 0.045 mm thick. Tensile samples approximately 3.5 mm wide by 50 mm long were cut from the sheet in both the longitudinal direction (parallel to the draw, or extrusion, direction) and the transverse direction. The samples were loaded to failure in a SMS laboratory scale tensile tester with a 250 N load cell with the strain being derived from crosshead displacement at a commanded displacement rate of 0.8 mm/s (2 in./min). The initial tensile modulus was taken as a secant modulus from the initial portion of the stress–strain curve. The first point used in calculating the modulus was taken at several Newtons of load, above the load take-up region, and the last point was taken at about 15 N of load, before the curve became significantly non-linear. Yield stress was determined at the point of zero slope on the stress–strain curve during monotonic loading. Fiberglass tape was used as loading tabs covering approximately 12 mm of both ends of the specimen to prevent premature breakage in the grips.

2.2. Dynamic mechanical analysis

Samples 10 mm wide by 60 mm long were cut from the center of the same extruded sheet used for the tensile experiments. Storage and loss modulus data were collected on a Dupont/TA Instruments 982 resonant frequency DMA at the Air Force Research Laboratory, Propulsion Directorate. All of the samples were of similar crystallinities (approximately 15%) determined by differential scanning calorimetry (DSC). The sheet specimens were mounted horizontally in film grips with a clamping distance of approximately 30 mm, the resonant frequencies of the samples at room temperature were ca. 12 Hz, and the tests were conducted from -150°C to 200°C at a heating rate of $2^\circ\text{C}/\text{min}$. The apparatus was calibrated according to manufacturer

specifications and a standard length correction factor was used for all samples [22].

2.3. Infrared spectroscopy

Thin polymer films were cast onto potassium bromide windows from dilute trifluoroethanol solution. The samples were dried at 70°C for several hours and the sample chamber was purged with nitrogen for 5 min before the spectra were collected. Infrared absorption spectra were collected on a Nicolet 55XC FT-IR Spectrometer.

2.4. NO_x exposure tensile tests

Samples approximately 13 mm wide by 80 mm long were cut from extruded sheet approximately 0.3 mm thick and fiberglass tape was used to protect the grip-ends of the specimens. The specimens were hung in an exposure chamber purged with dry nitrogen at room temperature into which 1 vol% (300 cm³) of NO₂ was introduced from a “lecture bottle” purchased from US Welding. After the exposure time elapsed, the samples were removed from the chamber and loaded to failure in an Instron load frame. Again, strains were calculated from crosshead displacement, yield points were determined at the point of zero slope on the stress–strain curve, and the moduli were taken as a least squares fit through the linear (low load) region of the stress–strain curve.

3. Results and discussion

The results of tensile experiments on both longitudinal and transversely oriented extruded sheet samples are summarized in Table 1. It was found that the initial room temperature modulus more than doubled with the incorporation of 5 wt% clay in the nanocomposite in a nearly linear relationship with clay content. The yield strength improves by 175% for longitudinally oriented samples. Somewhat stronger anisotropy is observed in the yield stress data than in the initial modulus data. There is a 13% difference between the longitudinal and transverse yield stresses for the 5 wt% clay material and only a 4% difference for the modulus values. The strain-to-failure decreases slightly at 5 wt% clay loading, but is unchanged at 2 wt% clay loading.

These data agree well with that reported by Kojima et al.

[3]. However, the room temperature modulus of the 5 wt% clay material for the current work is 1.25 times greater than that reported by the Toyota Researchers. The samples used by Kojima et al. were injection molded dog bones and therefore less well oriented by flow and draw during processing than the sheet samples used in the current research. The water content of their samples was not reported. Differences in degree of chain orientation and water content may account for the differences in the room temperature mechanical properties between the two data sets.

Differences in mechanical properties between the longitudinally and transversely oriented samples are not apparent until the 5 wt% clay loading level. While a draw ratio of 4 is not significant, the Toyota researchers have reported [1] and X-ray results confirm [23], that the clay lamellae readily orient in the flow direction during processing and that the nylon-6 polymer chains also preferentially orient in the flow direction in the nanocomposite materials. That the clay lamellae cause the nylon-6 polymer chains to orient preferentially in the flow direction is evidenced by the difference in the longitudinal and transverse mechanical properties of the 5 wt% nanocomposite compared to the nylon-6.

To determine if the enhancement of the mechanical properties is due to the stiffness of the clay or to a constraining effect by the clay lamellae on the nylon-6 chains, the data can be fit with a rule of mixtures and the properties of the clay calculated. Using a volume-fraction-weighted additive rule of mixtures fit to the experimental data and extrapolating to 100% clay content, the resulting modulus of the clay lamellae is roughly 58 GPa. A modulus of 178 GPa has been published for a mica-type silicate lamellae [24,25]. Also, amorphous silica glass has a modulus of roughly 72 GPa and aluminum oxide has a modulus of 380 GPa [26], making 178 GPa a reasonable value for a phyllosilicate layer. Since the modulus of the clay calculated from this data set is an order of magnitude smaller than that expected from the literature data, it is unlikely that the modulus reinforcement mechanism is related solely to the increased volume of high stiffness clay lamellae in the nanocomposites.

We then consider the possibility that the modulus improvements are due to the constraint of the polymer chains by their interaction with the clay surfaces. Employing this assumption, the modulus of the constrained region can be calculated. Nielsen [27] advocates the use of a power

Table 1
Tensile results

Material	Initial modulus (GPa)		Yield stress (MPa)		Failure strain (%)	
	Long	Trans	Long	Trans	Long	Trans
Nylon-6	1.20 ± 0.12 ^a	1.20 ± 0.14	43.9 ± 3.1	46.4 ± 2.6	264 ± 39	296 ± 48
2 wt% Clay	1.65 ± 0.09	1.64 ± .06	58.9 ± 1.9	56.6 ± 2.2	292 ± 49	295 ± 46
5 wt% Clay	2.43 ± 0.13	2.33 ± .10	76.1 ± 3.6	66.7 ± 3.0	255 ± 10	240 ± 27

^a Standard deviation for the five samples tested.

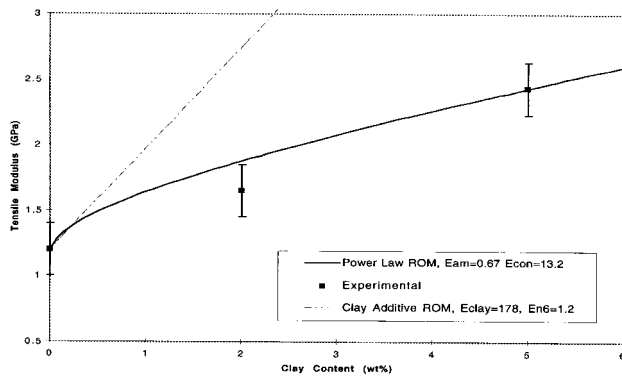


Fig. 1. Power law rule of mixing fit to predict experimental modulus values as a function of clay content.

law rule of mixing to predict the physical properties of polymer blends of two continuous phases: $P^n = P_1^n V_1 + P_2^n V_2$. Using strengths-of-materials arguments, Davies [28] derived an exponent of $1/5$, $n = 0.2$, for the shear modulus using this mixing rule. The modulus of the amorphous phase in nylon-6 has been determined to be approximately 0.8 GPa [29] in specially treated fibers and has been estimated to be as low as 0.3 GPa in the bulk polymer [30]. The volume fraction of polymer in the constrained region can be calculated [3] independently from loss and storage modulus data. Assuming the modulus of the amorphous region from the literature, the power law mixing rule can be applied to estimate the modulus of the constrained volume that best fits the experimental data. The results of this calculation are illustrated in Fig. 1. Iterating to fit the power law rule of mixing to the experimental data results in a modulus of 0.67 GPa for the amorphous volume fraction and 13.2 GPa for the constrained region, assuming no direct reinforcement from the clay lamellae. This estimate of the constrained volume modulus is an order of magnitude larger than the estimate of the amorphous volume modulus and is

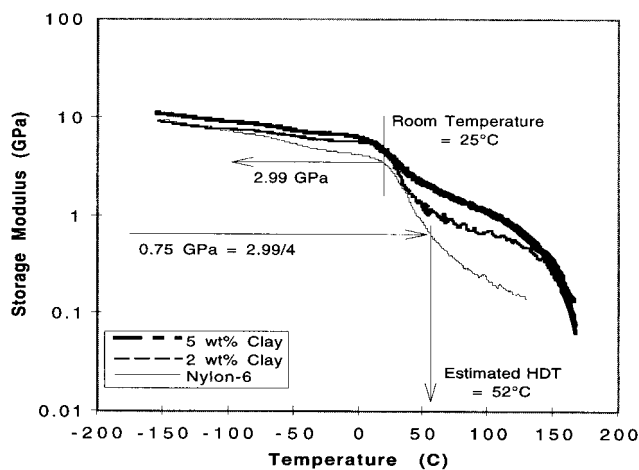


Fig. 2. Resonant frequency elastic spectra for nylon-6 and clay nanocomposites.

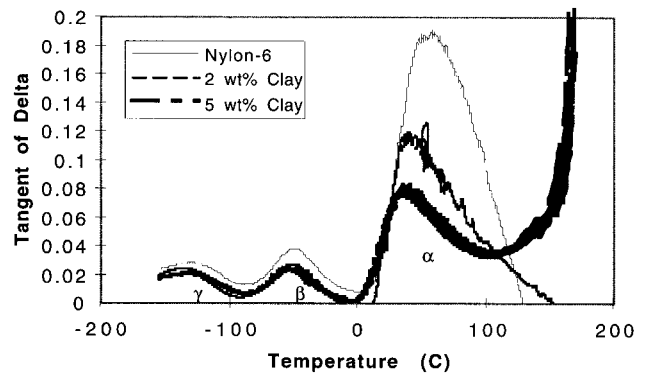


Fig. 3. Resonant frequency loss function for nylon-6 and clay nanocomposites.

of the same order of magnitude as the clay modulus that was calculated through the volume fraction weighted average rule of mixtures. However, 13 GPa is an order of magnitude smaller than the predicted modulus of nylon-6 crystal lamellae [27] of 100–300 GPa. It is plausible that if the interaction with the clay lamellae constrains the movement of the nylon-6 chains without confining the chains through long range order, the modulus of the constrained region should fall between the moduli for the wholly unrestrained chains of the amorphous region and the wholly restrained chains of the crystalline region.

The volume fraction of polymer in the constrained region is estimated by comparing the magnitudes of the alpha loss tangent peak, measured using DMA [3], with that of a sample of known constrained volume. The storage modulus and loss tangent temperature dependencies for nylon-6 and the clay nanocomposites are shown in Figs. 2 and 3, respectively. The method of constrained volume calculation used was developed by Oka and Chikahisa [31] to determine the crystallinities of semicrystalline polymers based on their DMA responses. The magnitude of the loss modulus at the peak of the alpha transition as a fraction of the total material response is compared to the loss fraction of a sample of known crystallinity. Since the crystallinity of the material is unchanged with increasing clay content, the resulting ratio can be interpreted as the volume fraction of all the polymer chains constrained in the nanocomposites by both crystallinity and clay-polymer interactions. Fundamental to the constrained volume calculation is the assumption that the magnitude of the loss response is due only to the freeing of polymer chain motion within the amorphous phase. Since the tested samples were all of similar crystallinities, as calculated from the areas under the heat flow versus temperature traces during the melt transition in DSC experiments, the decrease in the peak height with clay content is not due to a confinement of chains by increasing long range order. The constrained volumes calculated from the current data set agree with those published by Kojima et al. [3] for injection molded specimens.

The calculated constrained volume increases non-linearly

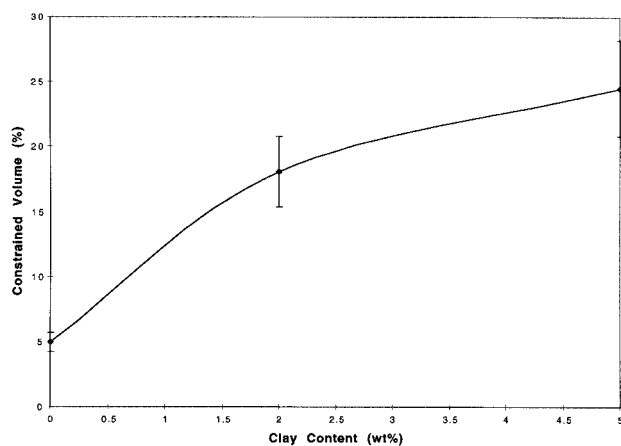


Fig. 4. Calculated constrained volume as a function of clay content.

with clay content, but correlates linearly with the increase in room temperature storage modulus of the nanocomposites materials, as shown in Figs. 4 and 5. This linear relationship suggests that it is the effect of constraining the polymer chains, not the volume fraction of the high modulus clay, which controls the improvement in room temperature storage modulus. The increase in estimated HDT (discussed later) for these materials adopts an exponential relationship with the increase in calculated constrained volume, as shown in Fig. 6.

HDT, was estimated from the storage modulus data as illustrated in Fig. 2. HDT values can be estimated within a sample set from DMA storage modulus data by determining the temperature at which the storage modulus drops to 25% of its room temperature value [32]. The decrease in the rate of decline of the storage modulus above $T = T_g$ also appears to increase with clay content. Similarly, Krishnamoorti and Giannelis [33] showed that the storage modulus of the nanocomposite materials increases with clay content in rheological experiments at 235°C. They also reported that the slope in the storage modulus versus frequency trace decreases with the addition of clay, essentially eliminating

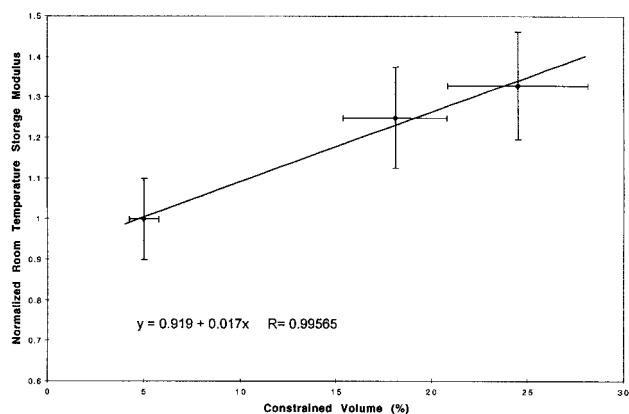


Fig. 5. Room temperature storage modulus as a function of calculated constrained volume.

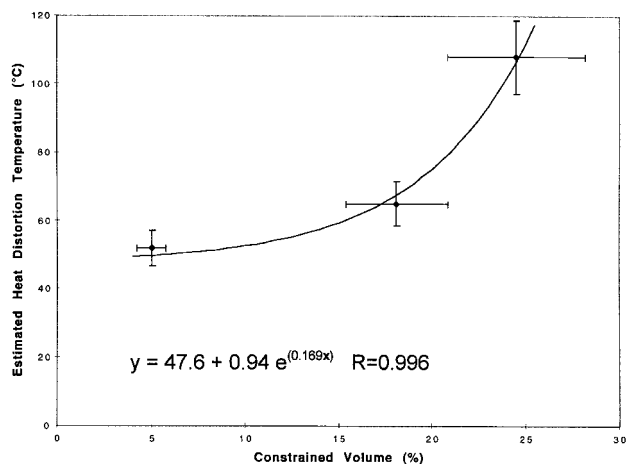


Fig. 6. Estimated HDT as a function of calculated constrained volume.

terminal behavior. This reported rheological effect is consistent with our observation of weaker temperature dependence of the storage modulus above the glass transition temperature. It is this weakening of the temperature dependence, not a change in the glass transition temperature, that is primarily responsible for the improvement in HDT that was reported by the Toyota researchers [3] and observed in our research.

As shown in Fig. 2, the magnitudes of the storage moduli are higher for the nanocomposites than for the unmodified nylon-6 throughout the temperature range. This increase in storage modulus agrees with the results of the tensile experiments discussed above, where the initial modulus at room temperature also increased with increasing clay content. However, it is interesting to note that the onset of the decrease in storage modulus occurs at lower temperatures with increasing clay content. The decrease in onset temperature for E' decay with clay content corresponds to a decrease in temperature of the maximum of the alpha transition in the loss tangent data, as shown in Fig. 3. DSC results also indicate a slight decrease in glass transition temperature with the addition of clay. The midpoint of the inflection of the heat flow versus temperature trace shifts from $39.9 \pm 2^\circ\text{C}$ for as-received nylon-6 to $37.5 \pm 2^\circ\text{C}$ for the 2 wt% clay nanocomposite. Since the onset of the decrease in storage modulus of a semi-crystalline polymer accompanies the glass transition, or the onset of long-range motion within the polymer chains in the amorphous region of the polymer [34], the decrease in onset temperature can be attributed to changes in the amorphous region of the nanocomposites due to the addition of clay. The exact nature of these changes remains unclear and is an aspect deserving further attention.

The behavior observed in the nanocomposite materials is curious because the crystallite size in the nanocomposites, studied by polarized light microscopy, is nearly an order of magnitude smaller than the spherulites observed in nylon-6 [20]. Smaller crystallites have more surface area for the

Table 2
Summary of dynamic mechanical data for nylon-6 nanocomposites

	Normalized storage modulus 25°C (GPa)	Calculated constrain volume (%)	Estimated HDT (°C)	Alpha peak location (°C)	Alpha peak mag	Beta peak location (°C)	Beta peak mag
Nylon-6	1	15	52	59.5	0.19	−46.9	0.038
2 wt% Clay	1.24	28	65	44.4	0.12	−51.1	0.027
5 wt% Clay	1.33	36	108	47.4	0.08	−51.6	0.024

same volume fraction and, therefore, would be expected to restrain movement of chains within the amorphous region more thoroughly than larger crystallites. More restraint of tie chains between crystallites would be expected to increase the temperature of the maximum of the alpha transition. However, Murayama [35] has shown that the temperature at which the glass transition occurs decreases at very large crystal volume fractions (about 50%). This decrease in T_g is attributed to an increase in the amorphous volume fraction due to the surface-to-volume ratio of the crystallites, the number of nuclei, and perfection of the crystal lamellae. The many small crystallites formed at high undercoolings restrain the amorphous region more thoroughly than the few large crystallites formed at higher crystallization temperatures, leading to the decrease in the temperature of the maximum of the alpha transition, or T_g , with very high crystal contents.

A similar argument can be used to explain the decrease in the maximum of the alpha transition in the nanocomposite materials. At 15% crystallinity, 36% of the polymer exists in the constrained region of the 5 wt% clay nanocomposite. A single constrained region may incorporate more than one crystallite, enclosing inter-crystallite tie chains, and having a smaller surface area than that of many small crystallites. Since the number of chains restrained by a crystallite (or by the constrained region) is proportional to the surface area, the reduction in the total surface area reduces the number of chains restrained by the constrained region when compared to multiple crystallites. With chains being restrained to a lesser extent, the activation energy for long-range chain motion decreases. Therefore, the temperature of both the onset and the maximum of the alpha transition of the loss tangent trace can be expected to decrease.

The concept of polymer chains being restrained from participating in relaxation mechanisms has been discussed for a number of other circumstances. Limitations on the kinetics of crystal growth [36], end-tethered polymer brushes [37], ionomer properties [38], and Wunderlich's rigid amorphous fraction [32] all rely on the concept of restraining the motion of polymer chains to explain the behavior of polymer systems. The constrained region concept has been explored by Eisenberg and co-workers for ionomers, or polymeric materials containing interactive ionic constituents. Eisenberg et al. [34] have reported, through model experiments with silica filler, that polymer chains can adsorb onto the surface of filler particles. Poly-

mer chains that interact with chains adsorbed to the filler surface are constrained from movement by this interaction. Constraining some of the polymer chains reduces the magnitude of the loss response in the material. When the constrained regions surrounding the filler particles are large enough to overlap, a second glass transition can be identified as a small, higher temperature, α' relaxation in the loss tangent trace.

A small secondary peak can be discerned in the loss tangent trace, Fig. 3, of the 5 wt% clay nanocomposite at approximately 145°C, well above the alpha transition (T_g) region. This secondary, α' , transition may be the glass transition of the nylon-6 chains in the constrained region, as explained by Eisenberg and Tsagaropoulos, or in the crystalline region, as explained by Takayanagi [39]. However, the crystallinity of these materials is approximately 15%. At this low volume fraction of crystallites, a separate α_c transition due to chain motion within the crystallites should not be observable. Therefore, it is more likely that the α' transition observed in the 5 wt% clay nanocomposite, and the broadening of the transition in the 2 wt% clay nanocomposite, is due to the onset of long-range motion within the constrained polymer chains. Following the Eisenberg explanation, 36% of the constrained volume due to either the clay surface interaction or crystallites is sufficient for the constrained regions to overlap.

Finally, with regard to the DMA observations, the beta transition in the loss tangent trace also becomes smaller in intensity and shifts to lower temperatures with the addition of clay for dry samples processed under the same conditions. The results shown in Fig. 3 and Table 2 suggest a decrease in carbonyl segment mobility with increasing clay content. This restriction of motion is expected if the mid-chain amide groups are constrained by the clay surfaces and well as the amine end groups [31].

The mechanism of the restraint of carbonyl segment mobility can be inferred from changes in the IR spectra. The infrared spectra indicate that the nylon-6 carbonyl units may be complexed with the clay surfaces, thereby reducing their mobility. The IR spectra of nylon-6 and nylon-6/5 wt% clay nanocomposite are shown in Fig. 7. The increase in absorption intensity at 1045 wavenumbers can be attributed to the Si–O stretch of the montmorillonite layers. There is an increased intensity and shift of the absorption peak to higher wavenumbers, from 3063 to 3095, in the region attributed to hydrogen bonded COOH

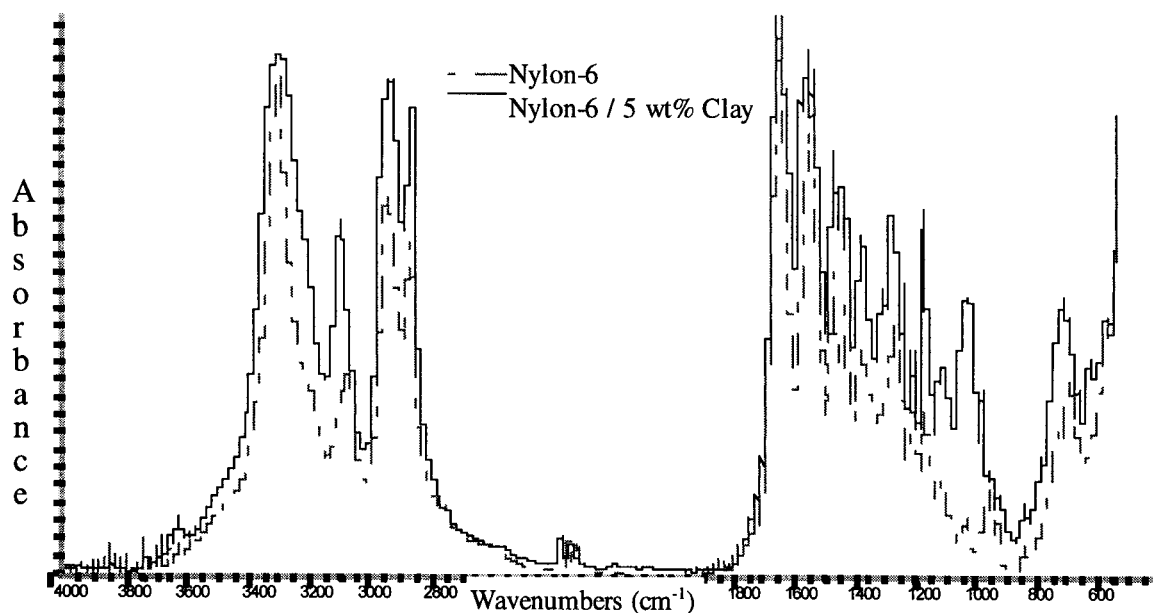


Fig. 7. IR spectra of nylon-6 and 5 wt% clay nanocomposite.

[40]. An increase and shift in the absorption peak at 700 wavenumbers is also evident. Absorption in the 700 wavenumbers region has been attributed to COOH deformation [41].

Shifts in the 3060 region similar to those observed in Fig. 7 have been attributed to the conversion of the nylon-6 mer unit from the *trans* conformation to the *cis* conformation by Dunn and Sansom [42]. An increase in intensity of the low frequency shoulder on the 3300 cm^{-1} N–H stretch accompanies the transformation to the *cis* isomer. Several more subtle changes in the IR spectra with the addition of clay resemble changes seen in nylon-6 complexed with metal halides [43,44]. Shifting of the amide I and II peaks, normally at 1635 and 1540 cm^{-1} , respectively, towards each other was noted by Dunn and Samson [40] and More and Donald [41]. Movement of the amide I peak is not apparent in the nanocomposite materials studied here. However, there is a broadening apparent on the higher frequency side of the 1540 cm^{-1} amide II peak. An additional peak appearing at 1595 cm^{-1} is also observed. This 1595 cm^{-1} peak is attributed to the formation of a metal complex with the oxygen atom of the carbonyl group and a change from *inter* molecular hydrogen bonding to *intra* molecular bonding in the literature. The nanocomposite materials crystallize into the gamma phase [1,23] and these changes in FTIR spectra of nylon-6 have been attributed to changes in crystal phase from alpha to gamma [45]. Therefore, the IR results both confirm the nylon-6/clay nanocomposite preference of the gamma crystal phase and suggest a mechanism for the constraining the nylon-6 polymer chains by complexation with the clay lamellae.

The complexation mechanism is similar to that which reportedly enables the crystal phase transformation from

alpha to gamma by soaking in aqueous potassium iodide [46]. Iodide has been shown, by Dunn and Samson [42], to form complexes with *N,N* dimethylacetamide, shifting the amide I stretch. The proposed crystal phase transformation mechanism is that I^{5-} ions complex with the carbonyl oxygens. This weakens the hydrogen bonds between the chains, possibly converting the chains to a *cis* configuration. The driving force for hydrogen bonding then twists the crystalline chains to the gamma phase. The complexation of the nylon chain with the negatively charged surface of the clay lamellae may similarly distort the conformation of the nylon-6 chains and form a complex with the carbonyl oxygens.

It can be hypothesized that, not only are the modified nylon-6 polymer chain ammonium end groups [3] tethered to the surface of the clay, but also the mid-chain carbonyl oxygens are complexed with the lamellae. Segments of the polymer chain are thereby immobilized, decreasing the number of chains participating in the glass transition. Therefore, the magnitude of the alpha transition decreases, as observed in Fig. 3. The complexation of the carbonyl oxygens may also interfere with the hydrogen bonding within the amorphous region, lowering the glass transition temperature.

The constrained volume helps to improve the tensile modulus and lower the permeability reported for the nanocomposite materials [47]. However, the incorporation of clay into the nylon-6 does little to protect the material from the effect of exposure to NO_x . While NO_2 is a pollutant monitored by the EPA, it exists as a variety of compounds in the atmosphere and is here referred to as NO_x . At standard atmosphere and pressure, NO_x is 29.5% NO_2 and 70.5% N_2O_4 [48]. HNO_3 and HNO_2 acids are formed by reaction

of NO_2 with water [49]. The results of residual strength tensile experiments on sheet samples exposed to NO_x are shown in Figs. 8–10. Both yield strength and initial modulus decrease nearly linearly with NO_x exposure time. While the strain-to-failure is relatively unaffected for nylon-6, it increases significantly for the nanocomposite materials after 10 h of exposure, but remains fairly constant thereafter.

NO_x is known to cause chain scission in nylon-6, decreasing molecular weight with exposure. Nitrogen dioxide reportedly attacks the nylon polymer chain and deprotonates the amide nitrogen in the carbonyl segment [50], causing chain scission at the weakest bond, the C–N bond [6]. The effects of declining molecular weight would be noticeable in the strain-to-failure data, but not in a linear relationship. So, the observed increase in strain-to-failure may be due to the declining molecular weight of the nylon-6.

Since the degree of degradation of nylon-6,6 shows an exponential decay with film thickness, Jellinek [48] concluded that the random chain scission process of NO_x attack was diffusion controlled. Smith [51] found that applied stress has a synergistic effect with NO_x in degrading the properties of highly oriented nylon-6 fibers. Strength decayed logarithmically with exposure time, as expected for a diffusion controlled process, but linearly with concentration. Unlike Jellinek's work on thin films of nylon-6,6, Igarashi determined that NO_x has negligible effect on the strength of unoriented rods of nylon-6 [52]. No change in modulus was detected for unoriented nylon-6 rods held for a week in an NO_x environment, regardless of the load on the sample up to 90% of ultimate tensile strength [53].

However, the current data show both initial modulus and yield stress decreasing linearly with exposure time. Since no effort was made to keep the experimental conditions rigorously anhydrous, it is likely that the degradation seen in these data is due not only to NO_2 attack, but also to solvation and attack by nitric acid. The reaction of NO_2 with water, either in the atmosphere or absorbed in the polymer, proceeds very quickly to acid formation. Perry discovered a tacky acidic layer on the surface samples exposed to NO_x for several hours [40]. A tacky surface layer was also

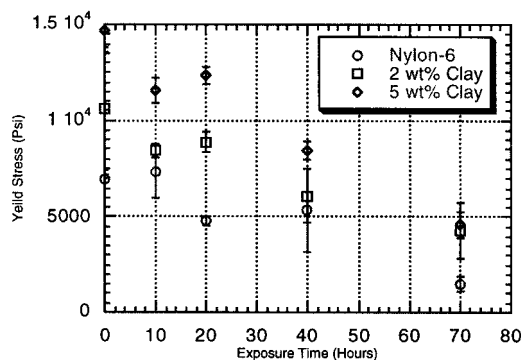


Fig. 8. Zero slope yield strength as a function of NO_x exposure time. Error bars indicate the standard deviation of five samples tested.

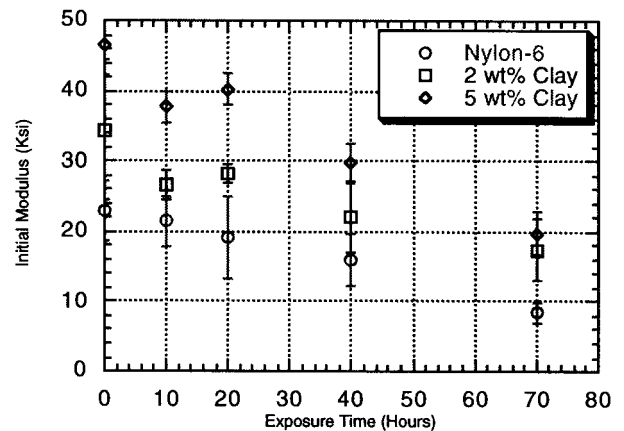


Fig. 9. Initial tensile modulus versus NO_x exposure time. Error bars indicate the standard deviation of five samples tested.

evident on the current samples that became more severe with increasing exposure time.

Strong acids dissolve nylons; and while nitric acid is not specifically listed as a solvent for nylon-6, it is a solvent for nylon-3 [54]. Solvation interrupts the inter-chain hydrogen bonding and dissociates the molecules from one another, leading to a stress cracking response. Hydrolysis of nylon-6 amides is also possible under acidic conditions [55]. Water protonates the amide group permitting exchange of the amide and hydroxyl functionalities, also leading to chain scission and crosslinking. It is likely that all three mechanisms, NO_2 attack, hydrolysis, and solvation, are influencing the mechanical response of the nylon-6 and nanocomposite materials.

To determine if the clay or constrained volume in the nanocomposite materials offered any protection to the nylon-6 from the effects of NO_x , the modulus data was normalized to the dry, unexposed, modulus for each material. Normalization corrects for differences in initial moduli between the materials and the data are plotted in Fig. 11. The normalized data for all three materials fall along the same degradation-time line. Since no change in the rate of degradation with clay content or constrained volume can be determined, it is likely that the degradation

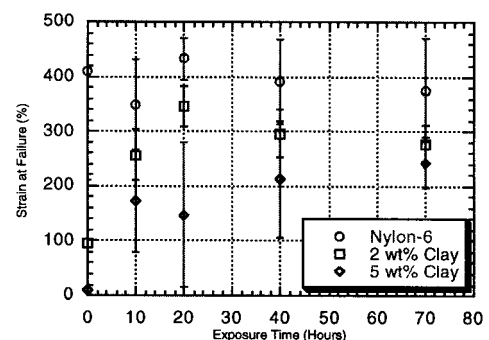


Fig. 10. Failure strain as a function of NO_x exposure time.

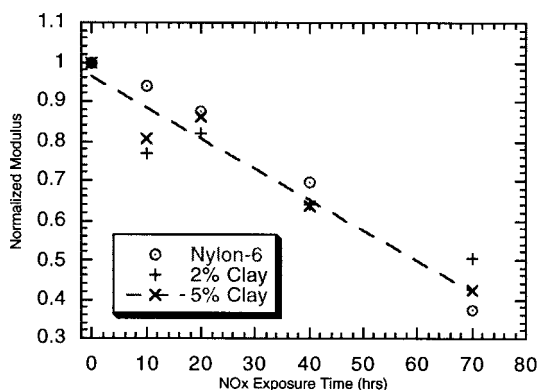


Fig. 11. Normalized modulus versus NO_x exposure time.

process is occurring in the amorphous regions of materials. Solvation is a diffusion limited process, and the crosslinking and chain scission caused by hydrolysis should be limited by the diffusion of the acidic environment. Shelley [23] has shown that the constrained volume both reduces the rate of diffusion and limits the total absorption of water in the nanocomposite materials to that which can be absorbed by the amorphous volume. Therefore, it is likely that the diffusion limited degradation processes are occurring in the amorphous region of the hybrid materials.

The mechanism of NO₂ attack is reported to be a free radical initiating process [50] that may not depend on NO₂ diffusion into the material. Since the NO_x degradation data do not show the characteristic exponential decay of a diffusion limited process, it is likely that the chemical kinetic free radical mechanism is influencing the loss of stiffness of the nylon-6 and nanocomposite materials. Since degradation experiments were conducted only at room temperature and 1 vol% NO_x concentration, an Arrhenius relationship of the strength degradation could not be explored. The change in degradation behavior with temperature is worthy of further research.

4. Conclusions

A 200% increase in tensile modulus and 175% improvement in yield stress is possible in extruded sheet of 5 wt% clay nanocomposite. While extrusion increases the anisotropy in the material, the difference between the longitudinal and transverse yield stresses are less than 15% for the 5 wt% clay nanocomposite with a processing draw ratio of 4. The improvement in mechanical properties correlates to an increase in the volume of polymer chains constrained by their interaction with the clay lamellae. The modulus of the polymer in the constrained region is an order of magnitude greater than that expected for amorphous nylon-6.

The constrained volume consists of polymer chains with their carbonyl segments complexed to clay lamellae along with ionic end group interactions. This mid-chain complexation reduces the effective number of chains participating in

glass transition as indicated by the reduction in magnitude of the alpha transition in the DMA data. A 63% decrease in the magnitude of the beta transition of the loss function indicates a significant reduction in the crankshaft motion of the carbonyl segments in the nylon-6 polymer chains.

The constraining effect of the clay lamellae does not protect the nanocomposites from NO_x attack. NO_x decreases the modulus and yield stress of moderately oriented nanocomposite sheet. The same rate of degradation occurs in the tensile modulus regardless of clay content or constrained volume.

Acknowledgements

Materials used in this research were graciously donated by Ube Industries. This research was sponsored by the NSF through grant CMS-9522743. The Polymer Working Group of the AFRL Propulsion Directorate provided time, equipment, and expertise. PTM acknowledges support from Air Force Office of Scientific Research under grant F49620-00-1-0100.

References

- [1] Kojima Y, Usuki A, Kawasumi M, Okada A, Fukushima Y, Kurauchi T, Kamigaito O. *J Mater Res* 1993;8:1185.
- [2] Kojima Y, Usuki A, Kawasumi M, Okada A, Fukushima Y, Kurauchi T, Kamigaito O. *J Appl Polym Sci* 1993;49:1259.
- [3] Usuki A, Koiwai A, Kojima Y, Kawasumi M, Okada AY, Kurauchi T, Kamigaito O. *J Appl Polym Sci* 1995;55:119.
- [4] Kojima Y, Usuki A, Kawasumi M, Okada A, Kurachi T, Kamigaito O. *J Polym Sci A* 1993;31:983.
- [5] Okada A, Usuki A, Kurauchi T, Kamigaito O. *Hybrid organic-inorganic composites*. Washington, DC: American Chemical Society, 1995 (p. 55).
- [6] DeVries KL, Perry MC. *Chemodegradation in polymer materials encyclopedia*. Boca Raton, FL: CRC Press, 1996 (p. 1187).
- [7] Kingery WD, Bowen HK, Uhlmann DR. *Introduction to ceramics*, 2nd ed.. New York: Wiley, 1976. p. 77–80.
- [8] Kojima Y, Usuki A, Kawasumi M, Okada A, Fukushima Y, Kurauchi T, Kamigaito O. *J Mater Res* 1993;8:1185.
- [9] US Patent # 2,951,087, 1960.
- [10] Friedlander HZ. *Polym Prepr* 1963;4:301.
- [11] US Patent # 4,739,007, 19 Apr 1988.
- [12] US Patent # 4,472,538, 18 Sep 1984.
- [13] Yang F, Ou Y, Yu Z. *J Appl Polym Sci* 1998;69:355.
- [14] Usuki A, Kato M, Okada A, Kurauchi J. *J Appl Polym Sci* 1997;63:137.
- [15] Hasegawa N, Kawasumi M, Kato M, Usuki A, Okada A. *J Appl Polym Sci* 1998;67:87.
- [16] Ke Y, Long C, Qi Z. *J Appl Polym Sci* 1999;71:1139.
- [17] Lee DC, Jang LW. *J Appl Polym Sci* 1996;61:1117.
- [18] Yono K, Usuki A, Okada A, Kurauchi T, Kamigaito O. *J Polym Sci, Polym Chem Ed* 1993;31:2493.
- [19] Lan T, Kaviratna PD, Pinnavaia TJ. *Chem Mater* 1994;6:573.
- [20] Messersmith PB, Giannelis EP. *J Polym Sci A: Polym Chem Ed* 1995;33:1047.
- [21] Wang MS, Pinnavaia TJ. *Chem Mater* 1994;6:468.
- [22] TA Instruments. *DMA calibration and data analysis program and operator's manual: 982 DMA, dynamic mechanical analyzer*. Dupont, 1983.
- [23] Shelley JS. PhD dissertation. University of Utah. In preparation.

- [24] Kornmann X, Berglund LA, Sterte J, Giannelis EP. *Polym Engng Sci* 1998;38:1351.
- [25] Powell B. Southern clay products. Personal communications, November 1999.
- [26] Kingery WD, Bowen HK, Uhlmann DR. *Introduction to ceramics*. 2nd ed.. New York: Wiley, 1976.
- [27] Nielsen LE. *J Appl Polym Sci* 1977;21:1579.
- [28] Davies WEA. *J Phys D* 1971;4:1176.
- [29] Prevorsek DC, Oswald HJ. Melt-spinning of PET and nylon fibers. In: Shultz JM, Fakirov S, editors. *Solid state behavior of linear polyesters and polyamides*. Englewood Cliffs, NJ: Prentice Hall, 1990 (chap. 3).
- [30] Shardakov IN, Matveyenko VP, Pistsov NV, Beghishev VP. *Polym Engng Sci* 1997;37:1270.
- [31] Oka S, Chikahisa Y. *Kobunshi Bussei*. Tokyo: Asakura Syoten, 1974 (p. 146).
- [32] Sepe MP. *Adv Mater Process* 1992;4:32.
- [33] Krishnamoorti R, Giannelis EP. *Macromolecules* 1997;30:4098.
- [34] Verma RK, Hsiao BS. *Trends Polym Sci* 1996;4:312.
- [35] Murayama T. *Dynamic mechanical analysis of polymeric materials*. New York: Elsevier, 1978.
- [36] Magill JH. *Polymer* 1962;3:655.
- [37] Fytas G, Anastasiadis SH, Seghrouchni R, Vlassopoulos D, Li J, Factor BJ, Theobald W, Toprakcioglu C. *Science* 1996;274:2041.
- [38] Tsagaropoulos G, Eisenberg A. *Macromolecules* 1995;28:6067–77.
- [39] Takayanagi M. *Viscoelastic properties of crystalline polymers*. Mem of the Fac of Eng, vol. 23, 1963. p. 80.
- [40] Silverstein RM, Bassler GC. *Spectrometric identification of organic compounds*. 2nd ed.. New York: Wiley, 1967.
- [41] Pretsch E, Clerc T, Seibl J, Simon W. *Tables of spectral data for structure determination of organic compounds: chemical laboratory practice*. Berlin: Springer, 1981.
- [42] Dunn P, Sansom G. *J Appl Polym Sci* 1969;13:1657.
- [43] More AP, Donald AM. *Polymer* 1990;34:5093.
- [44] Wyzgoski MG, Navok GE. *J Mater Sci* 1987;22:1707.
- [45] Rotter G, Ishida H. *J Polym Sci B, Polym Phys* 1992;30:489.
- [46] Kohan MI. *Nylon plastics handbook*. New York: Hanser, 1995.
- [47] Kojima Y, Usuki A, Kawasumi M, Okada A, Kurauchi T, Kamigaito O. *Mater Life* 1993;5:13.
- [48] McCarthy RD, Steurer HU, Daily MC. *The thermodynamic properties of nitrogen tetroxide*. National Bureau of Standards, NBSIR, 86-3054, 1986. p. 55.
- [49] Perry MC. PhD dissertation. University of Utah, 1997.
- [50] Jellinek HHG. Reaction of polymers with pollutant gases. In: Jellinek HHG, editor. *Aspects of degradation and stabilization of polymers*. Amsterdam: Elsevier, 1978 (chap. 9, p. 431).
- [51] Smith LV. MS thesis. University of Utah, 1991.
- [52] Igarashi M. PhD dissertation. University of Utah, 1982.
- [53] DeVries KL, Murthy S, Igarashi M. ASME Utec 84-029, 84-wa/mats-27.
- [54] Fuchs O. Solvents and non-solvents for polymers. In: Brandrup J, Immergut EH, editors. *Polymer handbook*, 3rd ed. New York: Wiley, 1989 (p. 392).
- [55] Morrison RT, Boyd RN. *Organic chemistry*. 5th ed. Boston: Allyn and Bacon, 1987 (p. 871).